J Electroceram (2012) 29:62–70
DOI 10.1007/s10832-012-9741-4

Effect of Ba^{2+} – Sr^{2+} co-substitution on the structural and dielectric properties of Lead Titanate

P. P. Bardapurkar · N. P. Barde · D. P. Thakur · K. M. Jadhav · G. K. Bichile

Received: 18 November 2011 / Accepted: 14 May 2012 / Published online: 27 May 2012

Abstract Growing interest in developing new materials for device applications led to study of ferroelectric oxides in a wide range and variety of compositions. In the present work, polycrystalline samples of lead barium strontium titanate ($Pb_{1-x}Ba_{0.5x}Sr_{0.5x}TiO_3$) solid solution system have been synthesized. Phase formation studies and crystal structure analysis were carried out by X ray diffractometry at room temperature, which suggested formation of single phase compound with tetragonal structure up to x=0.8 and cubic structure for x=1.0. The XRD pattern has been analyzed by employing Rietveld method. The phase transition in the system was confirmed by Differential Scanning Calorimetry (DSC). Samples with $0.0 \leq x \leq 0.8$ are in ferroelectric state whereas with x=1.0 is found to be in paraelectric state at room temperature. Co-substitution of Ba^{2+} and Sr^{2+} into lead titanate shows reduction in anisotropy as well as porosity. The dielectric studies of the system as a function of temperature and frequency were carried out in the range 323 K to 773 K and 100 Hz to 1 MHz respectively. Variation of dielectric constant and loss tangent with temperature shows peaking effect near Curie temperature. Frequency dependant dielectric studies clearly show that the dielectric constant and loss tangent decrease exponentially with increased frequency.

Keywords Ferroelectrics · X ray diffraction · Anisotropy · Dielectric response

P. P. Bardapurkar (✉)
S.N. Arts, D.J. Malpani Commerce & B. N. Sarda Science College,
Sangamner, M.S., India
e-mail: pranavbardapurkar@yahoo.com

N. P. Barde
Badrinarayan Barwale Mahavidyalaya,
Jalna, M.S., India

D. P. Thakur
School of Physical Sciences, Swami Ramanand Teerth Marathwada University,
Nanded, M.S., India

K. M. Jadhav · G. K. Bichile
Dr. Babasaheb Ambedkar Marathwada University,
Aurangabad, M.S., India

1 Introduction

Varieties of ferroelectric ceramics are being developed to suite the desired applications in a wide range, with a variety of chemical compositions. Among many ferroelectric materials, oxide materials with perovskite structure of general formula ABO_3 (A: mono or divalent ions, B: tri or hexa valent ions) are currently gaining interest of academicians and scientists due to their potential applications in the field of multilayer capacitors, piezoelectric actuators, infrared detectors, informatics, microwave domain, etc. [1–6]

Perovskite structure has been one of the most versatile structures for tailoring the properties of materials. From the family of perovskite structured ferroelectrics, $A^{2+}B^{4+}O_3$ type compounds that contain Ti^{4+}, solid solutions of Barium-Strontium Titanate, Lead-Barium Titanate, Lead-Strontium Titanate have been investigated extensively [7, 8]. Perovskite materials based on lead titanate ($PbTiO_3$-PT) are especially relevant as functional layers in piezoelectric, ferroelectric, pyroelectric and other devices and are found to emerge as materials of great importance due to their rich physical properties [9]. Recently lot of efforts have been taken to synthesize PT based bulk samples and thin films; and are extensively studied by modifying their properties with various techniques,

employing suitable method of preparation, selecting appropriate substitution of cations etc.; for variety of applications.

Lead Titanate (PT), Barium Titanium ($BaTiO_3$-BT) and Strontium Titanate ($SrTiO_3$-ST) forms a complete series of solid solutions [6] resulting in various potential materials like Barium Strontium Titanate (BST), Lead Barium Strontium Titanate (PST), and Lead Barium Titanate (PBT); with a perovskite structure. Among perovskite ferroelectric systems, PT, BT, ST, BST, PST, and PBT have been well studied by many researchers [10]. Literature discloses that the substitution of Ba^{2+} in PT reduces the lattice anisotropy and lead to different microstructure resulting in different dielectric behavior [7, 8]. Similarly, Sr^{2+} substitution in PT offers a good control over dielectric and piezoelectric properties, Curie temperature, lattice anisotropy, grain segregation etc. [4, 6, 11–13]. Thus, it is revealed from literature reports that, substitution of Ba^{2+} and Sr^{2+} into PT strongly influences properties of PT. However, to our knowledge, the influence of co-substitution of Ba^{2+} and Sr^{2+} which may overcome the difficulties in the synthesis [11], may lead to moderate dielectric properties and operating temperature close to the ambient temperature as required for many applications [14] is hardly reported in the literature. Hence from scientific and technological importance point of view, the present work has intuition to carry out a detailed study of effect of co-substitution of equal amounts of Ba^{2+} and Sr^{2+} into PT, on its structural, electrical and dielectric properties. In the present paper, we report our results on structural and dielectric properties of ($Pb_{1-x}Ba_{0.5x}Sr_{0.5x}TiO_3$ – PBST) system with $0.0 \leq x \leq 1.0$.

2 Experimental

Polycrystalline samples of ($Pb_{1-x}Ba_{0.5x}Sr_{0.5x}TiO_3$) ($0.0 \leq x \leq 1.0$) were prepared by solid-state reaction technique. All the chemicals used were of high purity grade (99.9 % pure). The starting materials; Lead Oxide (PbO), Barium Carbonate ($BaCO_3$), Strontium Carbonate ($SrCO_3$) and Titanium Dioxide (TiO_2) were mixed in stoichiometric proportion to obtain samples of PBST system with $0.0 \leq x \leq 1.0$. The constituent compounds; in suitable stoichiometry; were thoroughly mixed in an agate mortar for 2 h. The mixed materials were then calcined in a platinum crucible at 1023 K for 4 h. In order to compensate the Pb/PbO loss, 5 % (by weight) excess PbO was added. The calcined powders were sieved through a 200 mesh sieve and sintered at 1073 K for 6 h in air. Using a hydraulic press, the sintered fine powder was cold pressed into cylindrical pellets of diameter 10 mm and thickness 1–2 mm with a pressure of 6×10^7 kgm^{-2}. The pellets were finally sintered at temperatures varying from 1273 K to 1423 K for different compositions, in covered platinum crucibles for 4 h.

Formation of the compound was confirmed by X-ray diffractometry. The X-ray diffraction pattern (XRD) of the samples were recorded on sintered powders over a wide range of Bragg angle 2θ ($20° \leq 2\theta \leq 70°$) with a scanning rate of $2°min^{-1}$ at room temperature using Philips PW 1830 diffractometer with CuK_α radiation (1.5418 Å). For electrical characterization, the sintered discs were polished to make both the faces flat and parallel. These discs were electroded with high purity air-drying silver paste on both sides and then fired at 473 K for 2 h.

The differential scanning calorimetry measurements on typical samples (x=0.0, 0.4 and 1.0) were carried out in the temperature range 300 to 800 K. The temperature of the sample was raised at 10°C per minute.

Measurements of dielectric constant (ε) and loss tangent (tanδ) of the compounds were carried out using HP 4284-A LCR meter, both as a function of frequency (100 Hz–1 MHz) and temperature (323 K–773 K).

3 Results and discussion

3.1 Structural

Figure 1 shows the X-ray diffractograms of the ceramic system $Pb_{1-x}Ba_{0.5x}Sr_{0.5x}TiO_3$ for x=0.0, 0.2, 0.4, 0.6, 0.8 and 1.0. One can see that the samples are essentially in single phase form within the instrumental error. The XRD patterns shows the reflections (001), (100), (101), (110), (111), (002), (200), (102), (201), (210), (112), (211), (202), (220) belonging to the tetragonal structure [15] for $0.0 \leq x \leq$

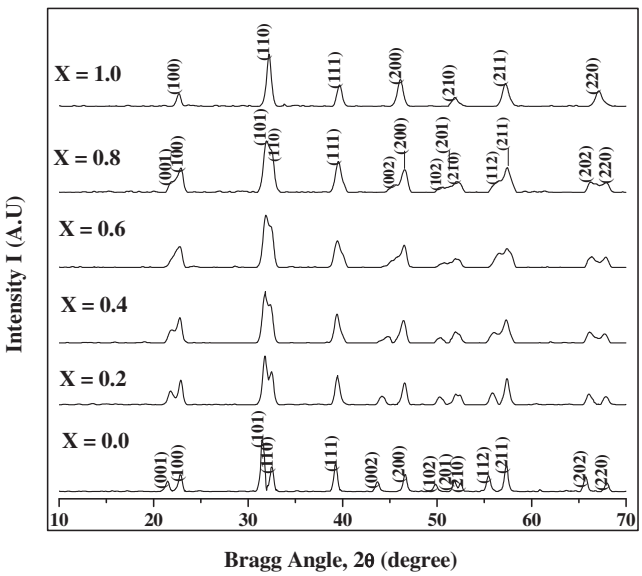

Fig. 1 XRD patterns for the $Pb_{1-x}Ba_{0.5x}Sr_{0.5x}TiO_3$ system (x=0.0, 0.2, 0.4, 0.6, 0.8 and 1.0)

0.8. For samples above x=0.8, only (100), (110), (200), (210), (211), (220) reflections corresponding to cubic phase are present. Thus, it is interesting to note that the structure changes from tetragonal to cubic for x=1.0 i.e. for $Ba_{0.5x}Sr_{0.5x}TiO_3$ in which Pb^{2+} ions are completely replaced by Ba^{2+} and Sr^{2+} ions in equal proportion.

All the observed peaks for $x \leq 0.8$ could be indexed to *P4mm* space group with tetragonal symmetry and show well correspondence with JCPDS card # 60452. For the x=1.0 composition, the XRD pattern was indexed to *Pm3m* space group having cubic structure and agrees well with JCPDS card # 391395. Typical diffractogram patterns; x=0.0 and x=0.2 were refined by Rietveld method. The refined XRD patterns for typical samples (x=0.0, 0.2) are shown in Fig. 2(a) and (b). The experimental points are plotted as circles (o) and theoretical data with a solid line. Difference between theoretical and experimental data is shown as the difference line at the bottom. The vertical lines represent the Bragg's allowed peaks. For Rietveld refinement, the XRD peaks were generated using *P4mm* space group i.e. in tetragonal symmetry and pseudo-Voigt function was used for the profile shape refinement. The refinement was carried out by allowing the variation of different parameters such as, cell parameters, scale factor, isotropic thermal parameters etc. The goodness of fit parameters for the refinements are found to be R_{wp}=29.9, R_{exp}=19.2, χ^2=1.14 for x=0.0 and R_{wp}=30.8, R_{exp}=24.2, χ^2=1.27 for x=0.2 composition.

The interplanar spacing (d) was calculated using the relation

$$\frac{1}{d^2} = \frac{h^2 + k^2}{a^2} + \frac{l^2}{c^2} \tag{1}$$

for tetragonal structure and using

$$\frac{1}{d^2} = \frac{h^2 + k^2 + l^2}{a^2} \tag{2}$$

for cubic structure. Table 1 gives observed and calculated values of interplanar spacing for the system, showing a good agreement.

It is reported that, when structure changes from tetragonal to cubic structure, reflections (101) and (110) collapse to a single reflection (110) [15]. In the present study, on co-substitution of Ba^{2+} and Sr^{2+} ions in place of Pb^{2+} ions, it is observed that, with increased substitution of $Ba^{2+}$and Sr Ba^{2+}, these reflections get merged into a single reflection. XRD patterns for the present system for 2θ=30° to 34° are presented in Fig. 3. A careful observation of Fig. 3 clearly indicates collapsing of (101) and (110) reflections into (110).

The other pairs of reflections observed in tetragonal x= 0.0 XRD pattern are also merged into single reflections, which indicates tetragonal to cubic transformation of the system as x changes from x=0.0 to x=1.0.

Using the XRD data, the lattice parameters of the ceramic system $Pb_{1-x}Ba_{0.5x}Sr_{0.5x}TiO_3$ were calculated with an accuracy of ±0.003 Å and the values are presented in Table 2. The variation of c/a ratio i.e. tetragonality as a function of composition is shown in Fig. 4. It is evident from Fig. 4 that, tetragonality decreases slowly as Ba^{2+}– Sr^{2+} composition increases from x=0.0 to x=0.8. The decrease in tetragonality may be attributed to substitution of average smaller ionic radius of Sr^{2+} ion. Figure 4 also gives the variation of unit cell volume of all the samples as a function of 'x'. It is observed from Fig. 4 that, like tetragonality, volume also decreases at much lower rate with increasing composition.

X-ray densities (ρ_X) of all the samples were calculated using the formula

$$\rho_X = \frac{\sum A}{NV} \tag{3}$$

Where ΣA is the sum of the atomic weight of all the atoms in the unit cell, V is volume of the unit cell and N is Avogadro's number [15]. The bulk density, ρ_B, was determined by Archimedes principle method. The values of ρ_X and ρ_B were used to calculate the percentage porosity using the relation [16]:

$$\%\ \text{porosity} = \frac{\rho_X - \rho_B}{\rho_X} \times 100 \tag{4}$$

The particle size of all the samples of the $Pb_{1-x}Ba_{0.5x}Sr_{0.5x}TiO_3$ system was estimated using Scherrer formula [15]. The most intense peak i.e. (101) for 0.0≤x≤0.8 and (110) for x=1.0, of XRD pattern was used to calculate the particle size. The values of ρ_X, $\rho_{B,\ \%}$ porosity and particle size obtained for the present samples are presented in Table 3.

Table 4 gives the Bragg's position and FWHM of the characteristic peak for the samples. Characteristic 100 % intensity peak width for all the compositions was compared. Composition with x=0.8 shows higher FWHM (0.57) than sample with x=0.6 (0.51) and sample with x=1.0 (0.45). Peak broadening increases from x=0.0 to 0.8 and suddenly decreases at x=1.0 (i.e. for $Ba_{0.5}Sr_{0.5}TiO_3$). This may be due to the compositional inhomogeneity, phase transition, presence of defects in the crystal lattice, etc. In the present case, the samples from x=0.0 to x=0.8 show tetragonal structure, whereas x=1.0 shows cubic structure. Thus the decrease in broadening from x=0.0 to x=1.0 may be attributed to this structural transformation [6].

All these studies reveal that the system has perovskite structure with Pb, Ba and Sr cations at 'A' site and 'Ti' anions at B site. 'A' site cations are surrounded by twelve 'O' anions in cubo-octahedral coordination; whereas the B site cations are situated in octahedral cavities defined by six anions. The pictorial representation of the structure is shown in Fig. 5.

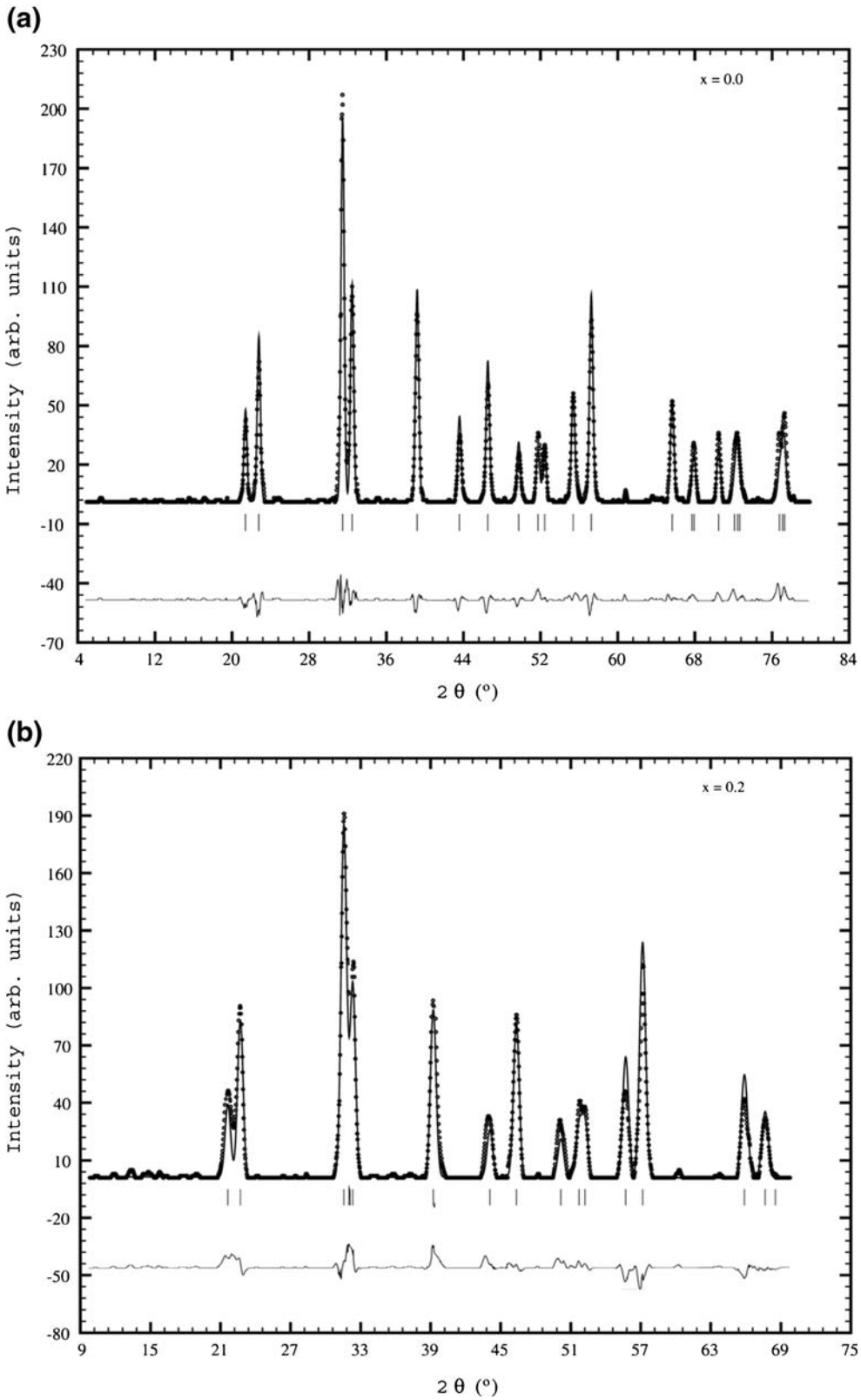

Fig. 2 (**a**) Rietveld refinement of typical sample x=0.0 of the $Pb_{1-x}Ba_{0.5x}Sr_{0.5x}TiO_3$ system. (**b**) Rietveld refinement of typical sample x=0.2 of the $Pb_{1-x}Ba_{0.5x}Sr_{0.5x}TiO_3$ system

Figure 6 shows typical Differential Scanning Calorimetry plots for samples x=0.0, 0.4 and 1.0. From these plots, it is evident that a dip near transition temperature is observed which diminishes as x varies from 0.0 to 1.0. A dip in the plots for x=0.0 and 0.4 indicates the ferroelectric to paraelectric transition temperature for these samples. The sample x=1.0 does not show any dip, indicating its T_c to be below room temperature and paraelectric nature at room temperature.

Table 1 Comparison of observed and calculated 'd' values for the $Pb_{1-x}Ba_{0.5x}Sr_{0.5x}TiO_3$ system

hkl		x=0.0	x=0.2	x=0.4	x=0.6	x=0.8	x=1.0
001	obs	4.1499	4.1232	4.1218	4.0736	4.0736	
	cal	4.1497	4.1147	4.1147	4.1415	4.1415	
100	obs	3.9047	3.9172	3.9141	3.8727	3.8727	3.9507
	cal	3.9045	3.9132	3.9132	3.8951	3.8951	3.9519
101	obs	2.8452	2.8341	2.8324	2.8066	2.8066	
	cal	2.8456	2.8356	2.8356	2.8373	2.8373	
110	obs	2.7593	2.7675	2.7658	2.7460	2.7460	2.7941
	cal	2.7590	2.7670	2.7670	2.7542	2.7542	2.7944
111	obs	2.2977	2.2937	2.2927	2.2767	2.2767	2.2802
	cal	2.2974	2.2961	2.2940	2.2934	2.2934	2.2816
002	obs	2.0742	2.0627	2.0598	1.9957	1.9957	
	cal	2.0747	2.0650	2.0530	2.0707	2.0707	
200	obs	1.9501	1.9568	1.9560	1.9447	1.9447	1.9753
	cal	1.9504	1.9566	1.9566	1.9475	1.9475	1.9759
102	obs	1.8312	1.8218	1.8212	1.8037	1.8037	
	cal	1.8316	1.8210	1.8210	1.8284	1.8284	
201	obs	1.7651	1.7664	1.7657	1.7566	1.7566	
	cal	1.7654	1.7670	1.7670	1.7624	1.7624	
210	obs	1.7440	1.7491	1.7484	1.7412	1.7412	1.7680
	cal	1.7445	1.7500	1.7494	1.7419	1.7419	1.7673
112	obs	1.6582	1.6519	1.6514	1.6295	1.6295	
	cal	1.6582	1.6510	1.6510	1.6551	1.6551	
211	obs	1.6080	1.6097	1.6093	1.6035	1.6035	1.6146
	cal	1.6084	1.6104	1.6104	1.6057	1.6057	1.6134
202	obs	1.4211	1.4178	1.4173	1.4113	1.4113	
	cal	1.4212	1.4178	1.4178	1.4169	1.4169	
220	obs	1.3795	1.3835	1.3845	1.3781	1.3781	1.3967
	cal	1.3794	1.3835	1.3842	1.3771	1.3771	1.3972

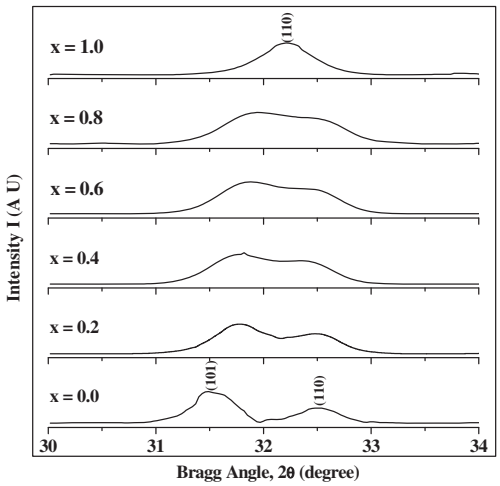

Fig. 3 XRD patterns for the $Pb_{1-x}Ba_{0.5x}Sr_{0.5x}TiO_3$ system for 2θ=30° to 34°

3.2 Dielectric Measurements

3.2.1 Temperature dependence

Figure 7 shows the variation of dielectric constant (ε) with temperature at a frequency of 1 kHz. From these plots, it can

Table 2 Lattice parameters for the PBST ceramics for the $Pb_{1-x}Ba_{0.5x}Sr_{0.5x}TiO_3$ system

Composition	Lattice Parameters	
x	a (Å)	c (Å)
0.00	3.9002	4.1489
0.20	3.9139	4.1047
0.40	3.911	4.103
0.60	3.909	4.101
0.80	3.905	4.105
1.00	3.952	3.952

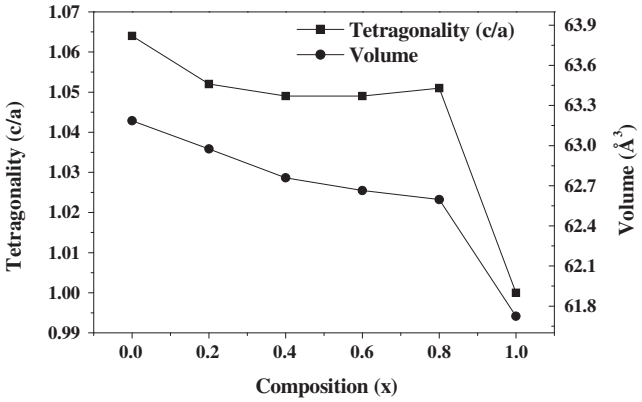

Fig. 4 Variation of tetragonality (c/a) and unit cell volume as a function of x for the $Pb_{1-x}Ba_{0.5x}Sr_{0.5x}TiO_3$ system

be seen that, the dielectric constant increases gradually with an increase in temperature up to transition temperature (T_c) and then decreases which indicates that samples have undergone a ferroelectric to paraelectric phase transition at the transition temperature. The temperature dependence of dielectric constant is almost similar at all the frequencies, but the increase in the value of dielectric constant with temperature is more pronounced at lower frequencies.

The dielectric polarization of a material comprises of electronic, ionic, space charge or interfacial and dipolar polarization. Electronic and ionic polarizations contribute to the dielectric constant at higher frequencies, whereas space charge and dipolar polarizations have their contribution at lower frequencies [4, 17, 18].

With the rise in temperature, the ionic distances get increased affecting electronic as well as ionic contributions and further get weakened with increase in temperature. The dipolar polarization is temperature dependant; decreases with rise in temperature whereas the interfacial polarization is frequency dependent and decreases with rise in the frequency. Interfacial polarization increases due to creation of crystal defects [18, 19].

In the present case, the rise in the dielectric constant with temperature up to the transition temperature may be attributed to the interfacial polarization dominating the dipolar polarization. With further rise in the temperature beyond the transition temperature (T_c), there is a rapid loss of polarization in the material. This loss in polarization results in monotonous fall of dielectric constant. The transition temperature is composition dependent and decreases systematically with increase of Sr^{2+} content as the addition of Sr^{2+} weakens the ferroelectric interaction. In the present study, it is observed that the transition temperature decreases with increasing $Ba^{2+} - Sr^{2+}$ content. For $x=1.0$, T_c is below room temperature (which is also reflected by the corresponding DSC plot, Fig. 6), the system is in paraelectric phase at room temperature, hence it does not show any dielectric maxima at and above ambient temperature.

The region around the dielectric maxima is broadened indicating the phase transition of diffused type. This can be explained on the basis of co-existence of the ferroelectric as well as paraelectric region in the vicinity of the transition temperature and is attributed to disorder in the arrangement of cations at 'A' site. The $Ba^{2+} - Sr^{2+}$ additives lead to a microscopic heterogeneity in the composition resulting in the distribution of different local Curie points. The diffuseness or peak broadening occurs mainly due to compositional fluctuations and/or substitution disordering of cation arrangement.

The first member of the system is $PbTiO_3$ which is ferroelectric at room temperature, tetragonal in structure and has high ferroelectric to paraelectric transition Curie temperature (763 K), whereas the end member of the system is $Ba_{0.5}Sr_{0.5}TiO_3$ which is paraelectric at room temperature,

Table 3 Theoretical density, experimental density, % porosity and particle size for the $Pb_{1-x}Ba_{0.5x}Sr_{0.5x}TiO_3$ system

x	ρ_{th} (g/cm^3)	ρ_{exp} (g/cm^3)	Porosity (%)	Particle Size (Å)
0.00	7.97	7.01	12	183
0.20	7.49	6.68	11	196
0.40	7.02	6.39	9	172
0.60	7.14	6.55	8	162
0.80	6.03	5.56	8	145
1.00	5.60	5.23	7	184

Table 4 Bragg Position of the prominent peak and FWHM for the $Pb_{1-x}Ba_{0.5x}Sr_{0.5x}TiO_3$ system

x	2θ (degree)	FWHM (degree)
0.00	31.46	0.37
0.20	31.56	0.42
0.40	31.59	0.48
0.60	31.62	0.51
0.80	31.67	0.58
1.00	32.00	0.45

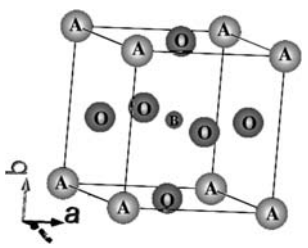

Fig. 5 Unit cell structure for the $Pb_{1-x}Ba_{0.5x}Sr_{0.5x}TiO_3$ system in which A: Pb^{2+}, Ba^{2+}, Sr^{2+}; B: Ti^{4+}

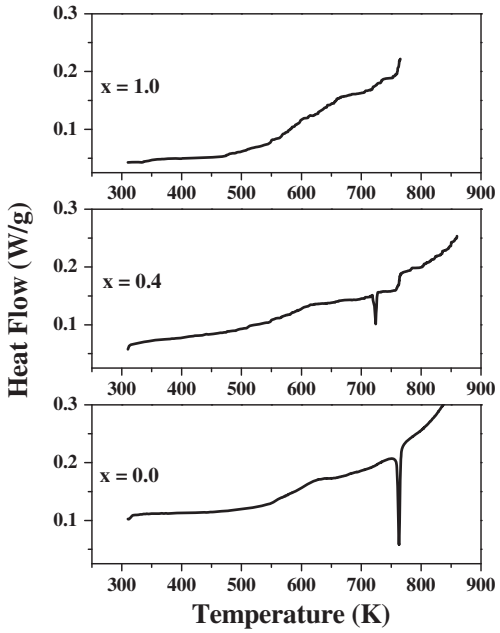

Fig. 6 Typical DSC plots for the samples x=0.0, 0.4, and 1.0 for the $Pb_{1-x}Ba_{0.5x}Sr_{0.5x}TiO_3$ system

cubic in structure and has low (below room temperature) Curie temperature. Hence as 'x' increases, there is systematic change in the structural arrangement also, the ferroelectric and paraelectric regions co-exist in the vicinity of transition temperature, leading to purely paraelectric material for x=1.0. Hence the dielectric maxima show a more diffused transition with increase of 'x'. Observations on the similar line are reported earlier [1].

Figure 8 shows variation of loss tangent with temperature at a frequency of 1 kHz. These plots exhibit a hump at a particular temperature which is close to the Curie temperature of the sample. Height of the hump decreases as Ba^{2+} – Sr^{2+} content increases. Such variations in tanδ also confirm phase transition in the samples [16]. At higher temperatures, the dielectric properties become dispersive due to higher losses at low frequency. The decrease of tanδ at the phase transition may be due to the reduction in the domain wall contribution to the loss. The dispersive loss at high temperatures is probably due to localized ionic conductivity [20].

3.2.2 Frequency dependence

Temperature dependent dielectric measurements reveal that the Curie temperature for the parent compound ($PbTiO_3$) is 763 K; whereas that for the end member of the series - BST—it is below room temperature. The co substitution of Ba^{2+} and Sr^{2+} gives the substituted system with a highest Curie temperature of 723 K. Thus, the frequency dependence of dielectric constant was studied at this temperature and is shown in Fig. 9. Dielectric constant is found to decrease with increasing frequency. The fall in dielectric constant arises from the fact that polarization does not take place instantaneously with the application of electric field due to inertia. The delay in response towards the impressed alternating electric field leads to loss and reduction in the dielectric constant [1]. As frequency is increased, samples with large relaxation time cease to respond and hence there is decrease in dielectric constant. Figure 10 shows variation of tanδ with frequency which

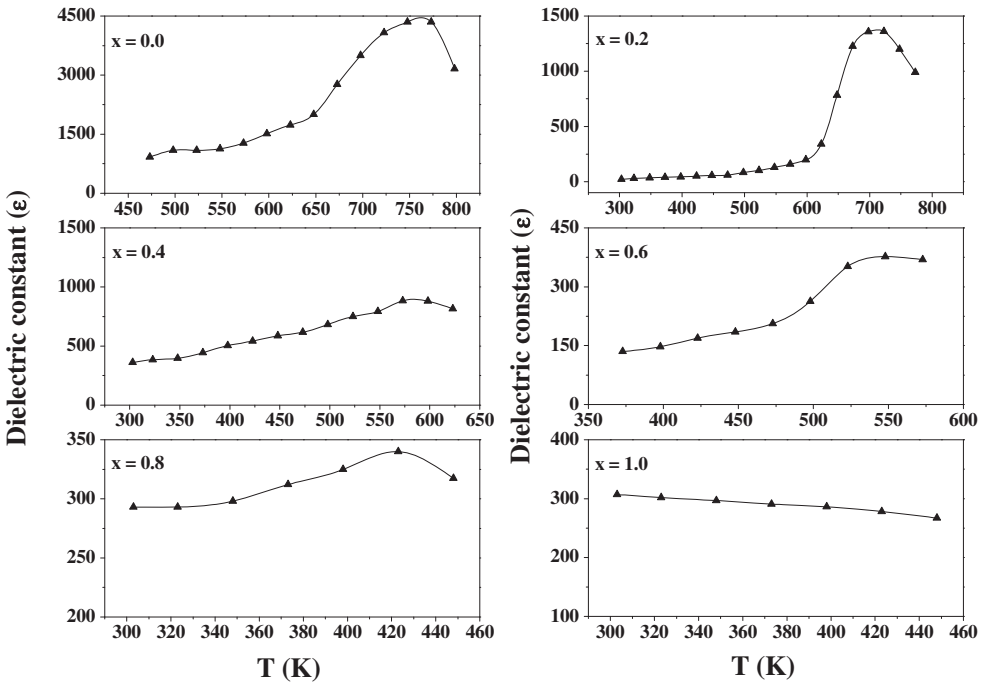

Fig. 7 Temperature dependence of dielectric constant (ε) at 1 kHz for the $Pb_{1-x}Ba_{0.5x}Sr_{0.5x}TiO_3$ system

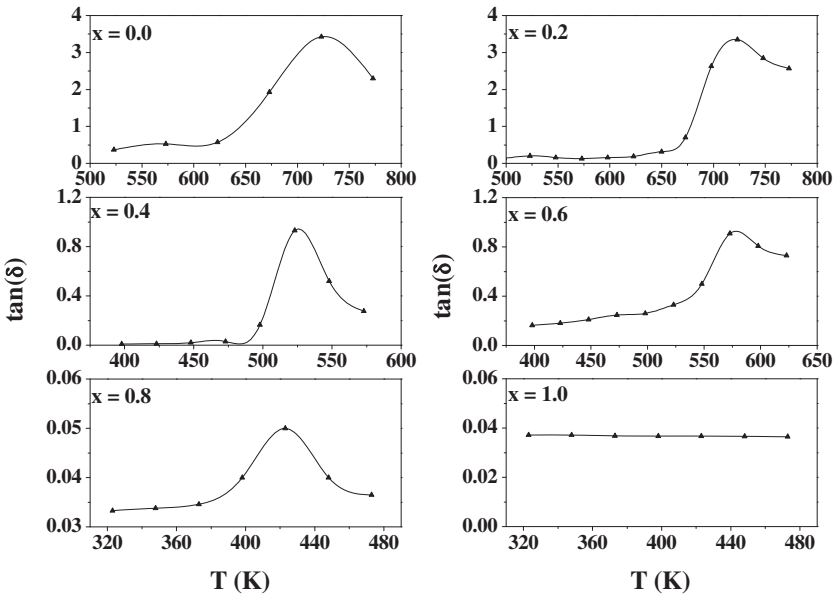

Fig. 8 Temperature dependence of loss tangent at a frequency of 1 kHz for the $Pb_{1-x}Ba_{0.5x}Sr_{0.5x}TiO_3$ system

shows that the values of tanδ decrease with increase in frequency. Such a trend of variations further reveals that the losses are the characteristic of the dipole mechanism [18].

4 Conclusions

Structural studies on the $Pb_{1-x}Ba_{0.5x}Sr_{0.5x}TiO_3$ system shows the strong effect of co-substitution of $Ba^{2+}$and Sr^{2+} on the properties of Lead Titanate. XRD patterns for x=0.0 to 0.8 suggests single phase formation. System has tetragonal structure for $x \leq 0.8$ and cubic for x=1.0. Samples with $x \leq 0.8$ are ferroelectric whereas sample x=1.0 is paraelectric above room temperature. Lattice anisotropy (c/a ratio) as well as porosity is found to decrease with increased Ba^{2+} – Sr^{2+} content. Variation of dielectric constant with temperature shows a hump about ferroelectric to paraelectric phase transition temperature. Similar behavior is observed for variation of tanδ. Dielectric constant of the system is almost constant at higher frequencies. With increase in frequency, tanδ decreases.

Thus, the co-substitution of Ba^{2+} – Sr^{2+} in PT ceramics reduces porosity, Curie temperature, anisotropy to sufficient value. The dielectric constant and dielectric loss tangent significantly get modified. These changes in the structural and dielectric properties by co-substitution of Ba^{2+} – Sr^{2+} may be useful for the applications in the field of transducers,

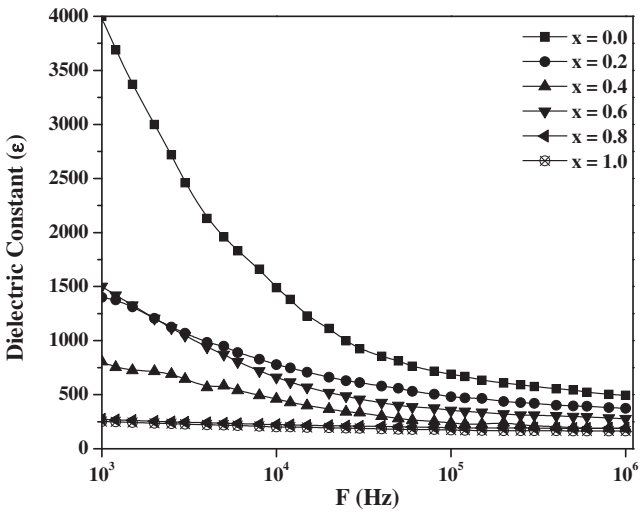

Fig. 9 Frequency dependence of dielectric constant (ε) at 723 K for the $Pb_{1-x}Ba_{0.5x}Sr_{0.5x}TiO_3$ system

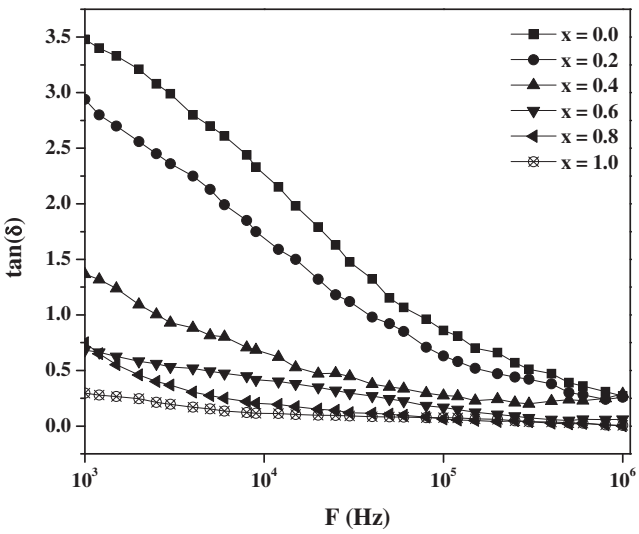

Fig. 10 Frequency dependence of loss tangent at 723 K for the $Pb_{1-x}Ba_{0.5x}Sr_{0.5x}TiO_3$ system

high frequency applications, informatics, piezoelectric actuators etc.

Acknowledgement PPB, NPB and DPT are thankful to Professor D.G. Kuberkar, Saurashtra University, Rajkot and Professor S.I. Patil, University of Pune, India for their invaluable guidance and fruitful discussions.

References

1. R. Rai, S. Sharma, N.C. Soni, R.N.P. Choudhary, Physica B **382**, 252 (2006)
2. H.R. Rukmini, R.N.P. Chaudhary, D.L. Prabhakara, Mater. Lett. **44**, 96 (2000)
3. C. Lei, K. Chen, X. Zhang, Mater. Sci. Eng. B **111**, 107 (2004)
4. H.V. Alexandru, C. Berbecaru, A. Ioachim, M.I. Toacsen, M.G. Banciu, L. Nedelcu, D. Ghetu, Mater. Sci. Eng. B **109**, 152 (2004)
5. S.W. Liu, Y. Lin, J. Weaver, W. Donner, X. Chen, C.L. Chen, J.C. Jiang, E.I. Meletis, A. Bhalla, Appl. Phys. Lett. **85**, 3202 (2004)
6. M. Jain, S.B. Mujumder, R. Guo, A.S. Bhalla, R.S. Katiyar, Mater. Lett. **56**, 692 (2002)
7. X. Sun, H. Huang, S. Wang, M. Li, Xing-zong Zhao, Thin Solid Films **516**, 1308 (2008)
8. K.-T. Kim, C.I. Kim, Thin Solid Films **420–421**, 544 (2002)
9. F.M. Pontes, S.H. Leal, E.R. Leite, E. Longo, P.S. Pizani, A.Z. Chiquito, J.A. Varela, J. Appl. Phys. **96–2**, 1192 (2004)
10. L. Radhapiyari, O.P. Thakur, C. Prakash, Mater. Lett. **57**, 1824 (2003)
11. T.-Y. Chen, S.-Y. Chu, Y.-D. Juang, Sens. Actuators A **102**, 6 (2002)
12. F. Zang, T. Karaki, M. Adachi, Powder Technol. **159**, 13 (2005)
13. D.H. Kang, J.H. Kim, J.H. Park, K.H. Yoon, Mater. Res. Bull. **36**, 265 (2001)
14. K.-T. Kim, C.-I. Kim, Thin Solid Films **447–448**, 651 (2004)
15. B.D. Cullity, *Elements of X ray diffraction*, 2nd edn. (Addison-Wesley Publishing Co. Inc, Massachusetts, 1956)
16. O.P. Thakur, C. Prakash, D.K. Agrawal, Mater. Sci. Eng. B **96**, 221 (2006)
17. L.L. Hench, J.K. West, *Principles of electronic ceramics* (Wiley, New York, 1990)
18. V. Gupta, K.K. Bamzai, P.N. Kotru, B.M. Wanklyn, Mater. Sci. Eng. B **130**, 163 (2006)
19. K. Amarendra Singh, T.C. Goel, R.G. Mendiratta, J. Appl. Phys. **91**, 6626 (2002)
20. B. Jaffe, W.R. Cook Jr., H. Jaffe, *Piezzoelectric ceramics* (Academic, London, 1971)